Korean J. Chem. Eng., **28**(2), 428-439 (2011)
DOI: 10.1007/s11814-010-0376-3

Electrospun nanofibers with application in nanocomposites

Mohammad Kanafchian, Masoomeh Valizadeh, and Akbar Khodaparast Haghi†

University of Guilan, P. O. Box 3756, Rasht, Iran
(*Received 3 June 2010 • accepted 15 July 2010*)

Abstract−The use of fine fiber has become an important design tool for filter media. Nanofibers-based filter media have some advantages such as lower energy consumption, longer filter life, high filtration capacity, easier maintenance, low weight rather than other filter media. The nanofibers-based filter media made up of fibers of diameter ranging from 100 to 1,000 nm can be conveniently produce by electrospinning technique. Common filter media have been prepared with a layer of fine fiber on typically forming the upstream or intake side of the media structure. The fine fiber increases the efficiency of filtration by trapping small particles, which increases the overall particulate filtration efficiency of the structure. Improved fine fiber structures have been developed in this study in which a controlled amount of fine fiber is placed on both sides of the media to result in an improvement in filter efficiency and a substantial improvement in lifetime. In the first part of this study, the production of electrospun nanofibers is investigated. In the second part, a different case studyis presented to show how they can be laminated for application as filter media. Response surface methodology (RSM) was used to obtain a quantitative relationship between selected electrospinning parameters and average fiber diameter and its distribution.

Key words: Biopolymers, Scanning Electron Microscope, Morphology, Proteins, Nanofibers, Statistical Analysis

INTRODUCTION

Polymeric nanofibers can be made by using the electrospinning process, as has already been described in the literature [1-10]. Electrospinning (Fig. 1) uses a high electric field to draw a polymer solution from the tip of a capillary toward a collector [16-20]. A voltage is applied to the polymer solution that causes a jet of the solution to be drawn toward a grounded collector. The fine jets dry to form polymeric fibers, which can be collected as a web [11-17].

In the nonwoven industry one of the fastest growing segments is in filtration applications. Traditionally wet-laid, melt blown and spun nonwoven articles containing micron size fibers are most popular for these applications because of the low cost, easy processability and good filtration efficiency. Their applications in filtration can be divided into two major areas: air filtration and liquid filtration (Fig. 2).

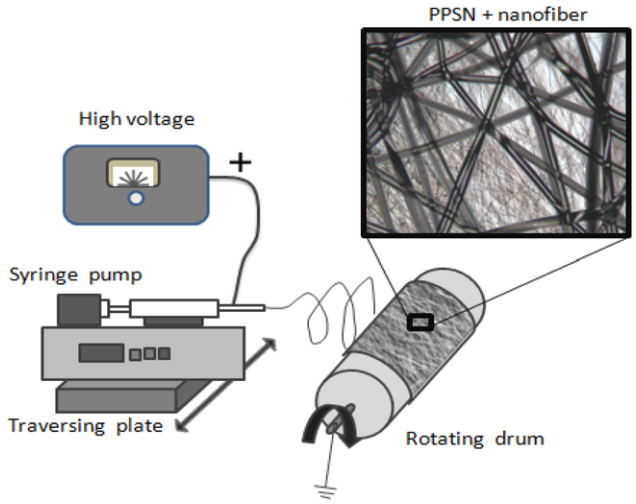

Fig. 1. Electrospinning setup.

Another type of electrospinning equipment (Fig. 2) also uses a variable high voltage power supply from Gamma High Voltage Research (USA). The applied voltage can be varied from 1-30 kV. A 5-ml syringe was used and positive potential was applied to the polymer blend solution by attaching the electrode directly to the outside of the hypodermic needle with internal diameter of 0.3 mm. The collector screen was a 20×20 cm aluminum foil, which was placed 10 cm horizontally from the tip of the needle. The electrode of opposite polarity was attached to the collector. A metering syringe pump from New Era pump systems Inc. (USA) was used. It was responsible for supplying polymer solution with a constant rate of 20 μl/min.

Electrospinning was done in a temperature-controlled chamber and the temperature of the electrospinning environment was adjusted on variable temperatures. A schematic diagram of the electrospinning apparatus is shown in Fig. 3.

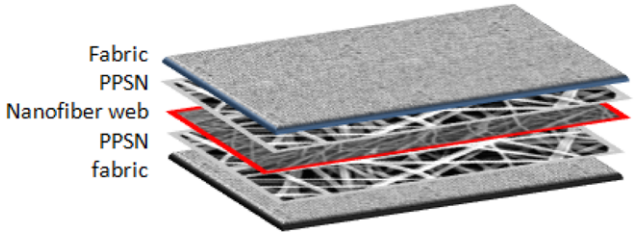

Fig. 2. Multilayer fabric components.

†To whom correspondence should be addressed.
E-mail: Haghi@Guilan.ac.ir

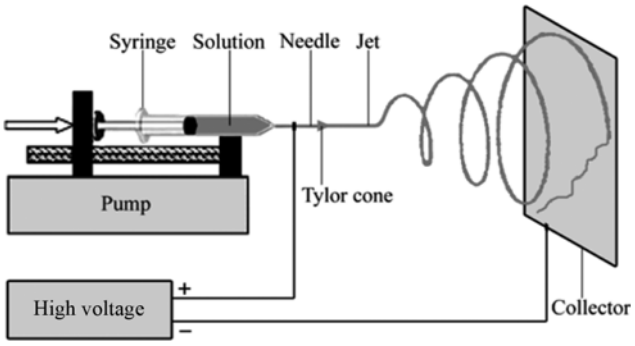

Fig. 3. Schematic diagram of a general type of electrospinning apparatus.

Electrospinning is a process that produces continuous polymer fibers with diameter in the submicron range. In the electrospinning process the electric body force acts on an element of charged fluid. Electrospinning has emerged as a specialized processing technique for the formation of sub-micron fibers (typically between 100 nm and 1 μm in diameter), with high specific surface areas. Due to their high specific surface area, high porosity, and small pore size, the unique fibers have been suggested as excellent candidates for use in filtration [18-22].

Air and water are the bulk transportation medium for transmission of particulate contaminants. The contaminants during air filtration are a complex mixture of particles. Most of them are usually smaller than 1,000 μm in diameter chemical and biological aerosols are frequently in range of 1-10 μm. The particulate matters may carry some gaseous contaminants. In water filtration the removal of particulate and biological contaminants is an important step. Nowadays, the filtration industry is looking for energy-efficient high performance filters for filtration of particles smaller than 0.3 μm and adsorbed toxic gases [23-30].

Nanofibrous media have low basis weight, high permeability, and small pore size that make them appropriate for a wide range of filtration applications. In addition, nanofiber membrane offers unique properties like high specific surface area (ranging from 1 to 35 m^2/g depending on the diameter of fibers), good interconnectivity of pores and the potential to incorporate active chemistry or functionality on nanoscale. In our study, to prepare the filters, a flow rate 1 μl/h for solution was selected and the fibers were collected on an aluminum-covered rotating drum (with speed 9 m/min) which was previously covered with a polypropylene spun-bond nonwoven (PPSN) substrate of 28 cm×28 cm dimensions; 0.19 mm thickness; 25 g/m^2 weight; 824 $cm^3/s/cm^2$ air permeability and 140 °C melting point (Fig. 2).

Structure characteristics of nanofibrous filtering media such as layer thickness fiber diameter, nanofiber orientation, representative pore size, and porosity dictate the filter properties and quality. Clearly, the properties of a nanofibrous media will depend on its structural characteristics as well as the nature of the component fibers; thus, it is desirable to understand and determine these characteristics. In this work we tried to identify the orientation distribution function (ODF) of nanofibers in nanofilter, and the fiber thickness distribution and porosity of nanofibrous media by using image processing algorithms.

1. Effect of Systematic Parameters on Electrospun Nanofibers

It has been found that morphology such as fiber diameter and its uniformity of the electrospun nanofibers are dependent on many processing parameters. These parameters can be divided into three main groups: a) solution properties, b) processing conditions, c) ambient conditions. Each of the parameters has been found to affect the morphology of the electrospun fibers.

2. Solution Properties

Parameters such as viscosity of solution, solution concentration, molecular weight of solution, electrical conductivity, elasticity and surface tension have an important effect on the morphology of nanofibers.

3. Viscosity

The viscosity range of a different nanofiber solution which is spinnable is different. One of the most significant parameters influencing the fiber diameter is the solution viscosity. A higher viscosity results in a large fiber diameter. Beads and beaded fibers are less likely to be formed for the more viscous solutions. The bead diameter becomes bigger and the average distance between beads on the fibers become longer as the viscosity increases.

4. Solution Concentration

In the electrospinning process, for fiber formation to occur a minimum solution concentration is required. As the solution concentration increases, a mixture of beads and fibers is obtained. The shape of the beads changes from spherical to spindle-like when the solution concentration varies from low to high levels. The fiber diameter increases with increasing solution concentration because of the higher viscosity resistance. Nevertheless, at higher concentration the viscoelastic force which usually resists rapid changes in fiber shape may result in uniform fiber formation. However, it is impossible to electrospin if the solution concentration or the corresponding viscosity become too high due to the difficulty in liquid jet formation.

5. Molecular Weight

Molecular weight also has a significant effect on the rheological and electrical properties such as viscosity, surface tension, conductivity and dielectric strength. It has been observed that too low molecular weight solution tends to form beads rather than fibers and high molecular weight nanofiber solution gives fibers with larger average diameter.

6. Surface Tension

The surface tension of a liquid is often defined as the force acting at right angles to any line of unit length on the liquid surface. By reducing surface tension of a nanofiber solution, fibers could be obtained without beads. The surface tension seems more likely to be a function of solvent compositions, but is negligibly dependent on the solution concentration. Different solvents may contribute different surface tensions. However, a lower surface tension of a solvent will not necessarily always be more suitable for electrospinning. Generally, surface tension determines the upper and lower boundaries of electrospinning window if all other variables are held constant. The formation of droplets, bead and fibers can be driven by the surface tension of solution, and lower surface tension of the spinning solution helps electrospinning to occur at lower electric field.

7. Solution Conductivity

There is a significant drop in the diameter of the electrospun nanofibers when the electrical conductivity of the solution increases. Beads

may also be observed due to low conductivity of the solution, which results in insufficient elongation of a jet by electrical force to produce uniform fiber. In general, electrospun nanofibers with the smallest fiber diameter can be obtained with the highest electrical conductivity. This indicates that the drop in the size of the fibers is due to the increased electrical conductivity.

8. Applied Voltage

In the case of electrospinning, the electric current due to the ionic conduction of charge in the nanofiber solution is usually assumed small enough to be negligible. The only mechanism of charge transport is the flow of solution from the tip to the target. Thus, an increase in the electrospinning current generally reflects an increase in the mass flow rate from the capillary tip to the grounded target when all other variables (conductivity, dielectric constant, and flow rate of solution to the capillary tip) are held constant. Increasing the applied voltage (*i.e.*, increasing the electric field strength) will increase the electrostatic repulsive force on the fluid jet, which favors the thinner fiber formation. On the other hand, the solution will be removed from the capillary tip more quickly as jet is ejected from Taylor cone. This results in the increase of the fiber diameter.

9. Feed Rate

The morphological structure can be slightly changed by changing the solution flow rate. When the flow rate exceeded a critical value, the delivery rate of the solution jet to the capillary tip exceeded the rate at which the solution was removed from the tip by the electric forces. This shift in the mass-balance resulted in sustained but unstable jet and fibers with big beads formation.

In the first part of this study, the production of electrospun nanofibers was investigated. In another part, a different case study was presented to show how nanofibers can be laminated for application in filter media.

EXPERIMENTS: CASE1-PRODUCTION OF NANOFIBERS

1. Preparation of Regenerated SF Solution

Raw silk fibers (B.mori cocoons were obtained from domestic producer, Abrisham Guilan Co., IRAN) were degummed with 2 gr/L Na_2CO_3 solution and 10 gr/L anionic detergent at 100 °C for 1 h and then rinsed with warm distilled water. Degummed silk (SF) was dissolved in a ternary solvent system of $CaCl_2/CH_3CH_2OH/H_2O$ (1 : 2 : 8 in molar ratio) at 70 °C for 6 h. After dialysis with cellulose tubular membrane (Bialysis Tubing D9527 Sigma) in H_2O for 3 days, the SF solution was filtered and lyophilized to obtain the regenerated SF sponges.

2. Preparation of the Spinning Solution

SF solutions were prepared by dissolving the regenerated SF sponges in 98% formic acid for 30 min. Concentrations of SF solutions for electrospinning were in the range from 8% to 14% by weight.

3. Electrospinning

In the electrospinning process, a high electric potential (Gamma High voltage) was applied to a droplet of SF solution at the tip (0.35 mm inner diameter) of a syringe needle, The electrospun nanofibers were collected on a target plate which was placed at a distance of 10 cm from the syringe tip. The syringe tip and the target plate were enclosed in a chamber for adjusting and controlling the temperature. A schematic diagram of the electrospinning apparatus is shown in Fig. 2. The processing temperature was adjusted at 25, 50 and 75 °C. A high voltage in the range from 10 kV to 20 kV was applied to the droplet of SF solution.

4. Characterization

An optical microscope (Nikon Microphot-FXA) was used to investigate the macroscopic morphology of electrospun SF fibers. For better resolving power, morphology, surface texture and dimensions of the gold-sputtered electrospun nanofibers were determined using a Philips XL-30 scanning electron microscope. A measurement of about 100 random fibers was used to determine average fiber diameter and their distribution.

EXPERIMENT: CASE2-PRODUCTION OF LAMINATED COMPOSITES

Polyacrylonitrile (PAN) of 70,000 g/mol molecular weight from Polyacryl Co. (Isfehan, Iran) was used with Dimethylformamide (DMF) from Merck to form a polymer solution 12% w/w after stirring for 5 h and staying overnight under room temperature. The yellow and ripened solution was inserted into a plastic syringe with a stainless steel nozzle 0.4 mm in inner diameter and then it was placed in a metering pump from World Precision Instruments (Sarasota, Florida, USA). Next, this set was installed on a plate which it could traverse to left-right along drum (Fig. 1). The flow rate 1 μl/h for solution was selected and the fibers were collected on an aluminum-covered rotating drum (with speed 9 m/min) which was previously covered with a polypropylene spun-bond nonwoven (PPSN) substrate of 28 cm×28 cm dimensions; 0.19 mm thickness; 25 g/m^2 weight; 824 $cm^3/s/cm^2$ air permeability and 140 °C melting point. The distance between the nozzle and the drum was 7 cm and an electric voltage of approximately 11 kV was applied between them. Electrospinning process was carried out for 8 h at room temperature to reach approximately web thickness 3.82 g/m^2. Then nanofiber webs were laminated into cotton weft-warp fabric with a thickness 0.24 mm and density of 25×25 (warp-weft) per centimeter to form a multilayer fabric (Fig. 2). Laminating was performed at temperatures 85, 110, 120, 140, 160 °C for 1 min under a pressure of 9 gf/cm^2.

Air permeability of multilayer fabric before and after lamination was tested by TEXTEST FX3300 instrument (Zürich, Switzerland). Also, in order to consider nanofiber morphology after hot-pressing, another laminating was performed by a non-stick sheet made of Teflon (0.25 mm thickness) instead one of the fabrics (fabric/pp web/nanofiber web/pp web/non-stick sheet). Finally, after removing the Teflon sheet, the nanofiber layer side was observed under an optical microscope (MICROPHOT-FXA, Nikon, Japan) connected to a digital camera.

RESULTS AND DISCUSSION

1. Effect of Silk Concentration

One of the most important quantities related to electrospun nanofibers is their diameter. Since nanofibers result from evaporation of polymer jets, the fiber diameters will depend on the jet sizes and the solution concentration. It has been reported that during the traveling of a polymer jet from the syringe tip to the collector, the primary jet may be split into different-sized multiple jets, resulting in differ-

ent fiber diameters. When no splitting is involved in electrospinning, one of the most important parameters influencing the fiber diameter is the concentration of the regenerated silk solution. The jet with a low concentration breaks into droplets readily and a mixture of fibers, bead fibers and droplets as a result of low viscosity is generated. These fibers have an irregular morphology with large variation in size; on the other hand jets with high concentration do not break up but travel to the grounded target and tend to facilitate the formation of fibers without beads and droplets. In this case, fibers became more uniform with regular morphology.

At first, a series of experiments were carried out when the silk concentration was varied from 8 to 14% at the 15 kV constant electric field and 25 °C constant temperature. Below the silk concentration of 8% as well as at low electric filed in the case of 8% solution, droplets were formed instead of fibers. Fig. 2 shows the morphology of the obtained fibers from 8% silk solution at 20 kV. The obtained fibers are not uniform. The average fiber diameter is 72 nm and a narrow distribution of fiber diameters is observed. It was found that continuous nanofibers were formed above a silk concentration of 8% regardless of the applied electric field and electrospinning condition. In the electrospinning of silk fibroin, when the silk concentration is more than 10%, thin and rod-like, fibers with diameters range from 60-450 nm were obtained.

There is a significant increase in mean fiber diameter with the increasing of the silk concentration, which shows the important role of silk concentration in fiber formation during the electrospinning process. The concentration of the polymer solution reflects the number of entanglements of polymer chains in the solution, thus solution viscosity. Experimental observations in electrospinning confirm that for forming fibers, a minimum polymer concentration is required. Below this critical concentration, application of electric field to a polymer solution results in electrospraying and formation of droplets to the instability of the ejected jet. As the polymer concentration is increased, a mixture of beads and fibers is formed. Further increase in concentration results in the formation of continuous fibers, as reported in this paper. It seems that the critical concentration of the silk solution in formic acid for the formation of continuous silk fibers is 10%.

Experimental results in electrospinning showed that with increasing the temperature of the electrospinning process, the concentration of polymer solution has the same effect on fibers' diameter at 25 °C.

There is a significant increase in mean fiber diameter with increasing of the silk concentration, which shows the important role of silk concentration in fiber formation during electrospinning. It is well known that the viscosity of polymer solutions is proportional to concentration and polymer molecular weight. For concentrated polymer solution, the concentration of the polymer solution reflects the number of entanglements of polymer chains, thus having considerable effects on the solution viscosity. At fixed polymer molecular weight, the higher polymer concentration results in higher solution viscosity. The jet from low viscosity liquids breaks up into droplets more readily and few fibers are formed, while at high viscosity, electrospinning is prohibited because of the instability flow caused by the high cohesiveness of the solution. Experimental observations in electrospinning confirm that for fiber formation to occur, a minimum polymer concentration is required. Below this critical concentration, the application of an electric field to a polymer solution results in electro spraying and formation of droplets to the instability of the ejected jet. As the polymer concentration is increased, a mixture of beads and fibers is formed. Further increase in concentration results in the formation of continuous fibers, as reported in this chapter. It seems that the critical concentration of the silk solution in formic acid for the formation of continuous silk fibers is 10% when the applied electric field is in the range of 10 to 20 kV.

2. Effect of Electric Field

It was already reported that the effect of the applied electrospinning voltage is much lower than the effect of the solution concentration on the diameter of electrospun fibers. To study the effect of the electric field, silk solution with the concentration of 10%, 12%, and 14% was electrospun at 10, 15, and 20 kV at 25 °C. At a high solution concentration, the effect of applied voltage is nearly significant. It is suggested that, at this temperature, higher applied voltage causes multiple jets formation, which would provide decreased fiber diameter.

As the results of this finding it seems that the electric field shows different effects on the nanofiber morphology. This effect depends on the polymer solution concentration and electrospinning conditions.

3. Effect of Electrospinning Temperature

One of the most important quantities related to electrospun nanofibers is their diameter. Since nanofibers result from the evaporation of polymer jets, the fiber diameters will depend on the jet sizes**.** The elongation of the jet and the evaporation of the solvent both change the shape and the charge per unit area carried by the jet. After the skin is formed, the solvent inside the jet escapes and the atmospheric pressure tends to collapse the tube-like jet. The circular cross section becomes elliptical and then flat, forming a ribbon-like structure. In this work we believe that ribbon-like structure in the electrospinning of SF at higher temperature is thought to be related to skin formation at the jets. With increasing the electrospinning temperature, solvent evaporation rate increases, which results in the formation of skin at the jet surface. Non-uniform lateral stresses around the fiber due to the uneven evaporation of solvent and/or striking the target make the nanofibers with circular cross-section to collapse into ribbon shape.

Bending of the electrospun ribbons was observed on the SEM micrographs as a result of the electrically driven bending instability or forces that occurred when the ribbon was stopped on the collector. Another problem that may be occurring in the electrospinning of SF at high temperature is the branching of jets. With increasing the temperature of the electrospinning process, the balance between the surface tension and electrical forces can shift so that the shape of a jet becomes unstable. Such an unstable jet can reduce its local charge per unit surface area by ejecting a smaller jet from the surface of the primary jet or by splitting apart into two smaller jets. Branched jets, resulting from the ejection of the smaller jet on the surface of the primary jet, were observed in electrospun fibers of SF. The axes of the cones from which the secondary jets originated were at an angle near 90° with respect to the axis of the primary jet.

To study the effect of electrospinning temperature on the morphology and texture of electrospun silk nanofibers, 12% silk solution was electrospun at various temperatures of 25, 50 and 75 °C. Results are shown in Fig. 5. Interestingly, the electrospinning of silk solution showed flat fiber morphology at 50 and 75 °C, whereas

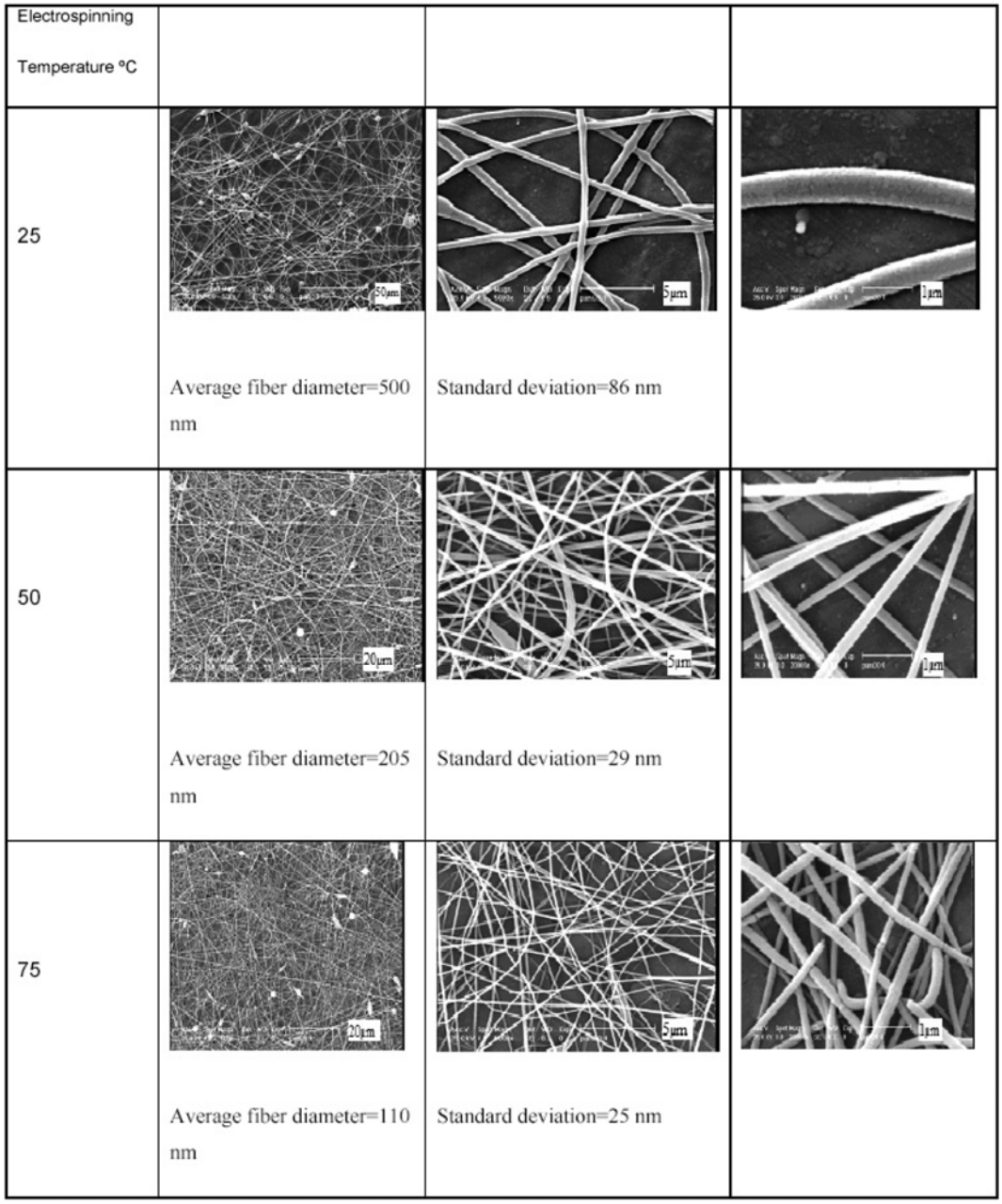

Fig. 4. SEM micrographs of electrospun nanofibers at applied voltage of 20 kV and PANI content of 20% with a constant spinning distance of 10 cm.

circular structure was observed at 25 °C. At 25 °C; the nanofibers with a rounded cross section and a smooth surface were collected on the target. Their diameter showed a size range of approximately 100 to 300 nm with 180 nm being the most frequently occurring. They are within the same range of reported size for electrospun silk nanofibers. With increasing the electrospinning temperature to 50 °C, the morphology of the fibers was slightly changed from circular cross section to ribbon-like fibers. Fiber diameter was also increased to a range of approximately 20 to 320 nm with 180 nm the most occurring frequency. At 75 °C, the morphology of the fibers was completely changed to ribbon-like structure. Furthermore, fiber dimensions were increased significantly to the range of 500 to 4,100 nm with 1,100 nm the most occurring frequency. The results are shown in Fig. 4.

EXPERIMENTAL DESIGN

Response surface methodology (RSM) is a collection of mathematical and statistical techniques for empirical model building (Appendix). By careful design of experiments, the objective is to optimize a response (output variable) which is influenced by several independent variables (input variables). An experiment is a series of tests, called runs, in which changes are made in the input variables in order to identify the reasons for changes in the output response.

To optimize and predict the morphology and average fiber diameter of electrospun silk, design of experiment was employed in the

Table 1. Central composite design

X_i	Independent variables	Coded values		
		−1	0	1
X_1	Silk concentration (%)	10	12	14
X_2	Applied voltage (KV)	10	15	20
X_3	Temperature (°C)	25	50	75

present work. Morphology of fibers and distribution of fiber diameter of silk precursor were investigated varying concentration, temperature and applied voltage. A more systematic understanding of these process conditions was obtained and a quantitative basis for the relationships between average fiber diameter and electrospinning parameters was established using response surface methodology (Appendix), which will provide some basis for the preparation of silk nanofibers.

A central composite design was employed to fit a second-order model for three variables. Silk concentration (X_1), applied voltage (X_2), and temperature (X_3) were three independent variables (factors) considered in the preparation of silk nanofibers, while the fiber diameters were dependent variables (response). The actual and corresponding coded values of three factors (X_1, X_2, and X_3) are given in Table 1. The following second-order model in X_1, X_2 and X_3 was fitted using the data in Table 1:

$$Y=\beta_0+\beta_1x_1+\beta_2x_2+\beta_3x_3+\beta_{11}x_1^2+\beta_{22}x_2^2+\beta_{33}x_3^2+\beta_{12}x_1x_2+\beta_{13}x_1x_3+\beta_{23}x_2x_3+\varepsilon$$

The Minitab and Mathlab programs were used for analysis of this second-order model and for response surface plots (Minitab 11, Mathlab 7).

By regression analysis, values for coefficients for parameters and P-values (a measure of the statistical significance) are calculated. When P-value is less than 0.05, the factor has significant impact on the average fiber diameter. If the P-value is greater than 0.05, the factor has no significant impact on the average fiber diameter. And R^2_{adj} (which represents the proportion of the total variability that has been explained by the regression model) for regression models was obtained (Table 2). The fitted second-order equation for average fiber diameter can be considered by:

$$Y=391+311\,X_1-164\,X_2+57\,X_3-162\,X_1^2+69\,X_2^2+391\,X_3^2 -159\,X_1X_2+315\,X_1X_3-144\,X_2X_3 \quad (1)$$

Where Y Average fiber diameter

Table 2. Regression analysis for the three factors (concentration, applied voltage, temperature) and coefficients of the model in coded unit*

Variables	Constant		P-value
	β_0	391.3	0.008
x_1	β_1	310.98	0.00
x_2	β_2	−164.0	0.015
x_3	β_3	57.03	0.00
x_1^2	β_{11}	161.8	0.143
x_2^2	β_{22}	68.8	0.516
x_3^2	β_{33}	390.9	0.002
x_1x_2	β_{12}	−158.77	0.048
x_1x_3	β_{13}	314.59	0.001
x_2x_3	β_{23}	−144.41	0.069
F	P-value	R^2	R^2 (adj)
18.84	0.00	0.907	0.858

*Model: $Y=\beta_0+\beta_1x_1+\beta_2x_2+\beta_3x_3+\beta_{11}x^2_1+\beta_{22}x^2_2+\beta_{332}x^2_3+\beta_{12}x_1x_2+\beta_{13}x_1x_3+\beta_{13}x_2x_3$ where "y" is average fiber diameter

From the P-values listed in Table 2, it is obvious that the P-value of term X_2 is greater than the P-values for terms X_1 and X_3. And other P-values for terms related to applied voltage such as, X_2^2, X_1X_2, X_2X_3 are much greater than the significance level of 0.05. That is, the applied voltage has not much significant impact on the average fiber diameter, and the interactions between concentration and applied voltage, temperature and applied voltage are not significant, either. But P-values for terms related to X_3 and X_1 are less than 0.05. Therefore, temperature and concentration have a significant impact on the average fiber diameter. Furthermore, R^2_{adj} is 0.858, so this model explains 86% of the variability in new data.

CONCLUSION

In the first parts of this study, the electrospinning of silk fibroin was processed and the average fiber diameters depend on the electrospinning condition. Morphology of fibers and distribution of diameter were investigated at various concentrations, applied voltages and temperature. The electrospinning temperature and the solution concentration have a significant effect on the morphology of the electrospun silk nanofibers. There effects were explained to be due to the change in the rate of skin formation and the evaporation rate

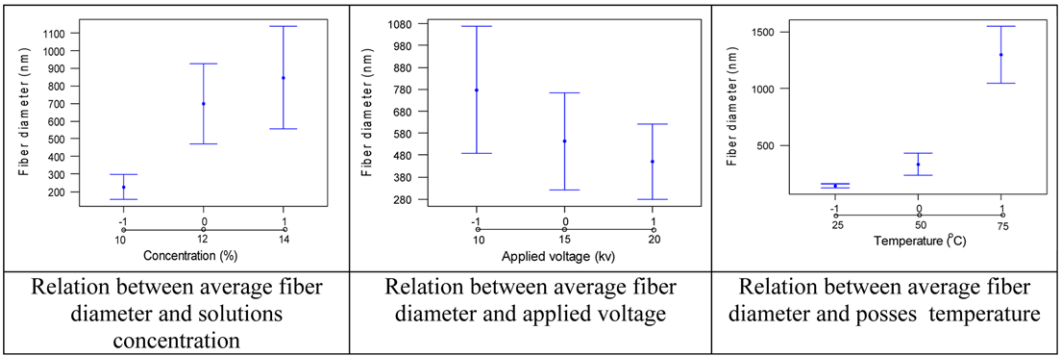

Fig. 5. Effect of electrospinning parameters on nanofibers diameter.

Laminating temperature (°C)	Taken images at 100 magnification	Observations
85	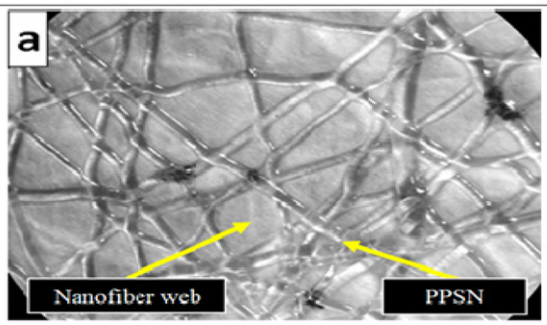	* Inconspicuous melting of PPSN
110	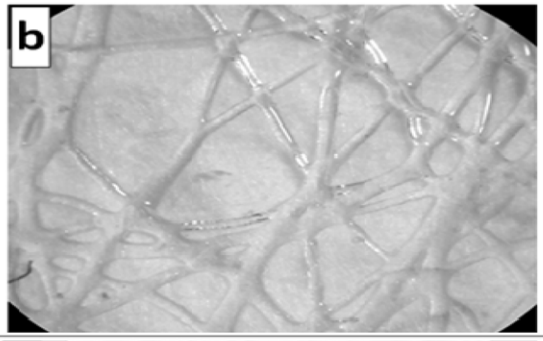	* Incomplete melting of PPSN and creation of linkage with nanofiber web
120	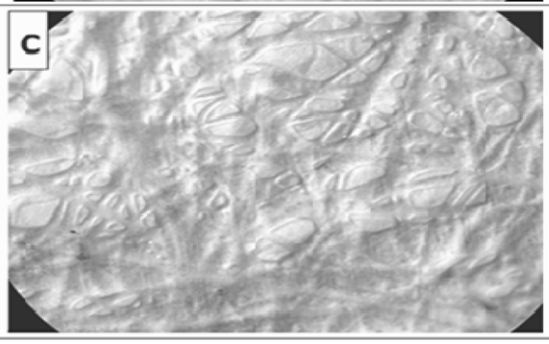	* Incomplete melting of PPSN and creation of linkage with nanofiber web * Spreading of melt over nanofiber surface because of pressing effect * Increasing junction area
140	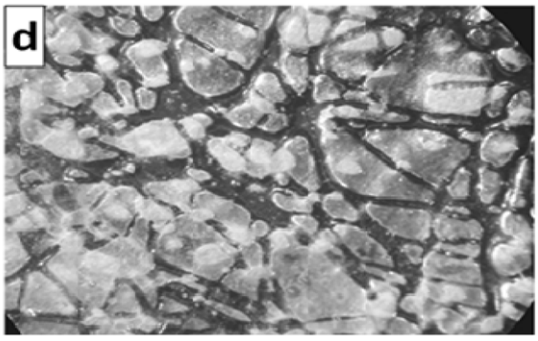	* Complete melting of PPSN with phase change * Penetration of melt into nanofiber web
160 (>140)	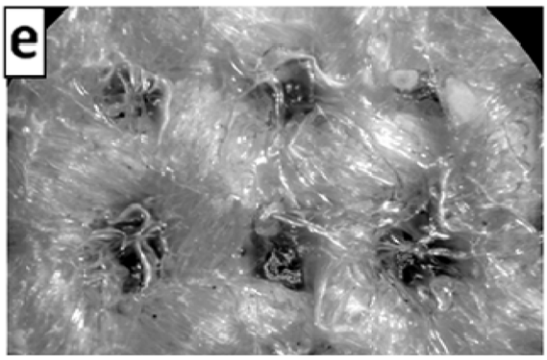	* Whole penetration of melt into nanofiber structure and web missing

Fig. 6. The optical microscope images of nanofiber web after lamination at various temperatures to be used as filter media.

of solvents. To determine the exact mechanism of the conversion of polymer into nanofibers requires further theoretical and experimental work.

From a practical view the results of the present work can be condensed. Concentration of regenerated silk solution was the most dominant parameter to produce uniform and continuous fibers. A jet with a low concentration breaks into droplets readily and a mixture of fibers and droplets as a result of low viscosity is generated. On the other hand, jets with high concentration do not break up but travel to the target and tend to facilitate the formation of fibers without beads and droplets. In this case, fibers become more uniform with regular morphology. In the electrospinning of silk fibroin, when the silk concentration is more than 10%, thin and rod-like fibers with diameters range from 60-450 nm were obtained. Furthermore, in the electrospinning of silk fibroin, when the process temperature was more than 25 °C, flat, ribbon-like and branched fibers with diameters ranging from 60-7,000 nm were obtained.

Two-way analysis of variance was carried out at the significance level of 0.05 to study the impact of concentration, applied voltages and temperature on average fiber diameter. It was concluded that concentration of solution and electrospinning temperature were the most significant factors impacting the diameter of fibers. Applied voltage had no significant impact on average fiber diameter.

In the second part of this study, the effect of laminating temperature on nanofiber/laminate properties is discussed. This laminating temperature is an important parameter to make next-generation filter media. Fig. 6 shows the optical microscope images of nanofiber web after lamination at various temperatures. We will discuss the laminating procedure in more detail in our future publications.

APPENDIX

Variables which potentially can alter the electrospinning process (Fig. A-1) are large. Hence, investigating all of them in the framework of one single research would almost be impossible. However, some of these parameters can be held constant during experimentation. For instance, performing the experiments in a controlled environmental condition, which is concerned in this study, the ambient parameters (i.e., temperature, air pressure, and humidity) are kept unchanged. Solution viscosity is affected by polymer molecular weight, solution concentration, and temperature. For a particular polymer (constant molecular weight) at a fixed temperature, solution concentration would be the only factor influencing the viscosity. In this circumstance, the effect of viscosity could be determined by the solution concentration. Therefore, there would be no need for viscosity to be considered as a separate parameter.

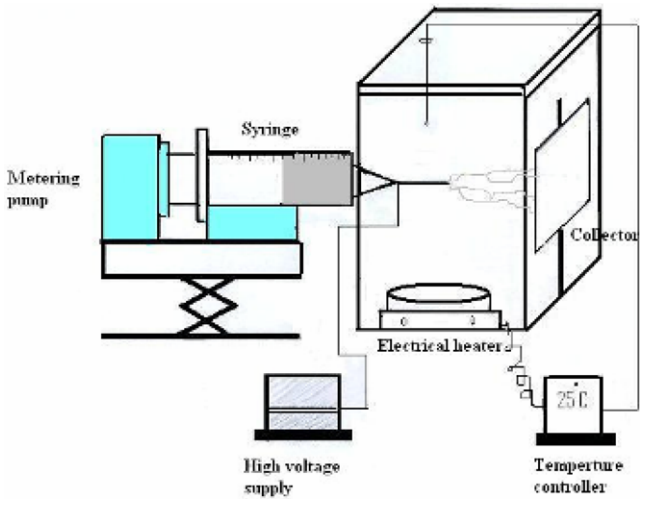

Fig. A-1. A typical image of electrospinning process.

In this regard, solution concentration (C), spinning distance (d), applied voltage (V), and volume flow rate (Q) were selected to be the most influential parameters. The next step is to choose the ranges over which these factors are varied. Process knowledge, which is a combination of practical experience and theoretical understanding, is required to fulfill this step. The aim is here to find an appropriate range for each parameter where dry, bead-free, stable, and continuous fibers without breaking up to droplets are obtained. This goal could be achieved by conducting a set of preliminary experiments while having the previous works in mind along with utilizing the reported relationships.

The relationship between intrinsic viscosity ($[\eta]$) and molecular weight (M) is given by the well-known Mark-Houwink-Sakurada equation as follows:

$$[\eta]=KM^{a} \quad \text{(A-1)}$$

where K and a are constants for a particular polymer-solvent pair at a given temperature. Polymer chain entanglements in a solution can be expressed in terms of Berry number (B), which is a dimensionless parameter defined as the product of intrinsic viscosity and polymer concentration ($B=[\eta]C$). For each molecular weight, there is a lower critical concentration at which the polymer solution cannot be electrospun.

As for determining the appropriate range of applied voltage, referring to previous works, it was observed that the changes of voltage lay between 5 kV to 25 kV, depending on experimental conditions; voltages above 25 kV were rarely used. Afterwards, a series of experiments were carried out to obtain the desired voltage domain. At $V<10$ kV, the voltage was too low to spin fibers and $10\text{ kV}\leq V<15$ kV resulted in formation of fibers and droplets; in addition, electrospinning was impeded at high concentrations. In this regard, $15\text{ kV}\leq V\leq 25$ kV was selected to be the desired domain for applied voltage.

The use of 5-20 cm for spinning distance was reported in the literature. Short distances are suitable for highly evaporative solvents, whereas it results in wet coagulated fibers for nonvolatile solvents due to insufficient evaporation time. Afterwards, this was proved by experimental observations and $10\text{ cm}\leq d\leq 20$ cm was considered as the effective range for spinning distance.

Few researchers have addressed the effect of volume flow rate. Therefore, in this case attention was focused on experimental observations. At $Q<0.2$ ml/h, in most cases especially at high polymer concentrations, the fiber formation was hindered due to insufficient supply of solution to the tip of the syringe needle. Whereas, excessive feed of solution at $Q>0.4$ ml/h incurred formation of droplets along with fibers. As a result, $0.2\text{ ml/h}\leq Q\leq 0.4$ ml/h was chosen as the favorable range of flow rate in this study.

Consider a process in which several factors affect a response of the system. In this case, a conventional strategy of experimentation,

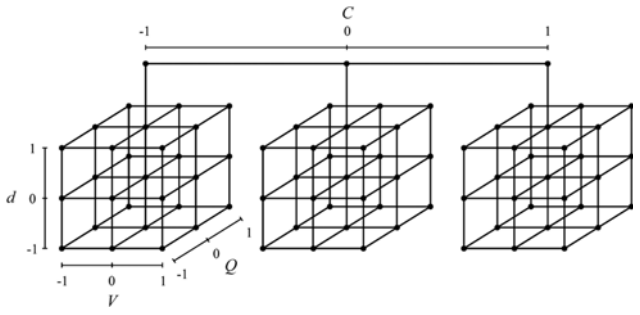

Fig. A-2. 3^4 Full factorial experimental design used in this study.

which is extensively used in practice, is the *one-factor-at-a-time* approach. The major disadvantage of this approach is its failure to consider any possible interaction between the factors, say the failure of one factor to produce the same effect on the response at different levels of another factor. For instance, suppose that two factors A and B affect a response. At one level of A, increasing B causes the response to increase, while at the other level of A, the effect of B totally reverses and the response decreases with increasing B. As interactions exist between electrospinning parameters, this approach may not be an appropriate choice for the case of the present work. The correct strategy to deal with several factors is to use a full factorial design. In this method, factors are all varied together; therefore, all possible combinations of the levels of the factors are investigated. This approach is very efficient, makes the most use of the experimental data and takes into account the interactions between factors.

It is trivial that in order to draw a line at least two points and for a quadratic curve at least three points are required. Hence, three levels were selected for each parameter in this study so that it would be possible to use quadratic models. These levels were chosen equally spaced. A full factorial experimental design with four factors (solution concentration, spinning distance, applied voltage, and flow rate) each at three levels (3^4 design) was employed resulting in 81 treatment combinations. This design is shown in Fig. A-2.

−1, 0, and 1 are coded variables corresponding to low, intermediate and high levels of each factor, respectively. The coded variables (x_j) were calculated using Eq. (A-2) from natural variables (ξ_j). The indices 1 to 4 represent solution concentration, spinning distance, applied voltage, and flow rate, respectively. In addition to experimental data, 15 treatments inside the design space were selected as test data and used for evaluation of the models. The natural and coded variables for experimental data (numbers 1-81) as well as test data (numbers 82-96) are listed in in the Appendix.

$$x_j = \frac{\xi_j - [\xi_{hj} + \xi_{lj}]/2}{[\xi_{hj} - \xi_{lj}]/2} \tag{A-2}$$

The mechanism of some scientific phenomena has been well understood and models depicting the physical behavior of the system have been drawn in the form of mathematical relationships. However, there are numerous processes at the moment which have not been sufficiently understood to permit the theoretical approach. Response surface methodology (RSM) is a combination of mathematical and statistical techniques useful for empirical modeling and analysis of such systems. RSM is applied in situations where several input variables are potentially influencing some performance measure or quality characteristic of the process - often called responses. The relationship between the response (y) and k input variables (ξ_1, ξ_2, …, ξ_k) could be expressed in terms of mathematical notations as follows:

$$y = f(\xi_1, \xi_2, \ldots, \xi_k) \tag{A-3}$$

where the true response function f is unknown. It is often convenient to use coded variables (x_1, x_2, …, x_k) instead of natural (input) variables. The response function will then be:

$$y = f(x_1, x_2, \ldots, x_k) \tag{A-4}$$

Since the form of true response function f is unknown, it must be approximated. Therefore, the successful use of RSM is critically dependent upon the choice of an appropriate function to approximate f. Low-order polynomials are widely used as approximating functions. First-order (linear) models are unable to capture the interaction between parameters which is a form of curvature in the true response function. Second-order (quadratic) models will likely perform well in these circumstances. In general, the quadratic model is in the form of:

$$y = \beta_0 + \sum_{j=1}^{k} \beta_j x_j + \sum_{j=1}^{k} \beta_{jj} x_j^2 + \sum_{i<j}^{k} \sum_{j=2}^{k} \beta_{ij} x_i x_j + \varepsilon \tag{A-5}$$

where ε is the error term in the model. The use of polynomials of higher order is also possible but infrequent. The βs are a set of unknown coefficients needed to be estimated. To do that, the first step is to make some observations on the system being studied. The model in Eq. (A-5) may now be written in matrix notation as:

$$\mathbf{y} = \mathbf{X}\beta + \varepsilon \tag{A-6}$$

where $\mathbf{y}$ is the vector of observations, $\mathbf{X}$ is the matrix of levels of the variables, β is the vector of unknown coefficients, and ε is the vector of random errors. Afterwards, method of least squares, which minimizes the sum of squares of errors, is employed to find the estimators of the coefficients ($\hat{\beta}$) through:

$$\hat{\beta} = (\mathbf{X}'\mathbf{X})^{-1}\mathbf{X}'\mathbf{y} \tag{A-7}$$

The fitted model will then be written as:

$$\hat{\mathbf{y}} = \mathbf{X}\hat{\beta} \tag{A-8}$$

Finally, response surfaces or contour plots are depicted to help visualize the relationship between the response and the variables and see the influence of the parameters. As one can notice, there is a close connection between RSM and linear regression analysis.

After the unknown coefficients (βs) were estimated by least squares method, the quadratic models for the mean fiber diameter (MFD) and standard deviation of fiber diameter (StdFD) in terms of coded variables were written as:

$$\begin{aligned} MFD = {} & 282.031 + 34.953x_1 + 5.622x_2 - 2.113x_3 + 9.013x_4 - 11.613x_1^2 \\ & - 4.304x_2^2 - 15.500x_3^2 - 0.414x_4^2 + 12.517x_1x_2 + 4.020x_1x_3 \\ & - 0.162x_1x_4 + 20.643x_2x_3 + 0.741x_2x_4 + 0.877x_3x_4 \end{aligned} \tag{A-9}$$

$$\begin{aligned} StdFD = {} & 36.1574 + 4.5788x_1 - 1.5536x_2 + 6.4012x_3 + 1.1531x_4 - 2.2937x_1^2 \\ & - 0.1115x_2^2 - 1.1891x_3^2 + 3.0980x_4^2 - 0.2088x_1x_2 + 1.0010x_1x_3 \\ & + 2.7978x_1x_4 + 0.1649x_2x_3 - 2.4876x_2x_4 + 1.5182x_3x_4 \end{aligned} \tag{A-10}$$

Table A-1. Summary of the results from statistical analysis of the models

	F	*p*-Value	R^2	R^2_{adj}	R^2_{pred}
MFD	106.02	0.000	95.74%	94.84%	93.48%
StdFD	42.05	0.000	89.92%	87.78%	84.83%

In the next step, several very important hypothesis-testing procedures were carried out to measure the usefulness of the models presented here. First, the test for significance of the model was performed to determine whether there is a subset of variables which contributes significantly in representing the response variations. The appropriate hypotheses are:

$$H_0: \beta_1=\beta_2=\cdots=\beta_k \quad \text{(A-11)}$$
$$H_1: \beta_j\neq 0 \text{ for at least one j}$$

The F statistics (the result of dividing the factor mean square by the error mean square) of this test along with the *p*-values (a measure of statistical significance, the smallest level of significance for which the null hypothesis is rejected) for both models are shown in Table A-1.

The *p*-values of the models are very small (almost zero); therefore, it could be concluded that the null hypothesis is rejected in both cases, suggesting that there are some significant terms in each model. Also included in are the values of R^2, R^2_{adj}, and R^2_{pred}. R^2 is a measure for the amount of response variation which is explained by variables and will always increase when a new term is added to the model regardless of whether the inclusion of the additional term is statistically significant or not. R^2_{adj} is the adjusted form of R^2 for the number of terms in the model; therefore, it will increase only if the new terms improve the model and decrease if unnecessary terms are added. R^2_{pred} implies how well the model predicts the response for new observations, whereas R^2 and R^2_{adj} indicate how well the model fits the experimental data. The R^2 values demonstrate that 95.74% of MFD and 89.92% of StdFD are explained by the variables. The R^2_{adj} values are 94.84% and 87.78% for MFD and StdFD, respectively, which account for the number of terms in the models. Both R^2 and R^2_{adj} values indicate that the models fit the data very well. The slight difference between the values of R^2 and R^2_{adj} suggests that there might be some insignificant terms in the models. Since the R^2_{pred} values are so close to the values of R^2 and R^2_{adj}, the models do not appear to be overfit and have very good predictive ability.

The second testing hypothesis is evaluation of individual coefficients, which would be useful for determination of variables in the models. The hypotheses for testing of the significance of any individual coefficient are:

$$H_0: \beta_j=0 \quad \text{(A-12)}$$
$$H_1: \beta_j\neq 0$$

The model might be more efficient with inclusion or perhaps exclusion of one or more variables. Therefore, the value of each term in the model is evaluated by using this test and then by eliminating the statistically insignificant terms, more efficient models could be obtained. The results of this test for the models of MFD and StdFD are summarized in Table A-2 and Table A-3, respectively. T statistic in these tables is a measure of the difference between an observed statistic and its hypothesized population value in units of standard error.

Table A-2. The test on individual coefficients for the model of mean fiber diameter (MFD)

Term (coded)	Coef.	T	*p*-Value
Constant	282.031	102.565	0.000
C	34.953	31.136	0.000
d	5.622	5.008	0.000
V	−2.113	−1.882	0.064
Q	9.013	8.028	0.000
C^2	−11.613	−5.973	0.000
d^2	−4.304	−2.214	0.030
V^2	−15.500	−7.972	0.000
Q^2	−0.414	−0.213	0.832
Cd	12.517	9.104	0.000
CV	4.020	2.924	0.005
CQ	−0.162	−0.118	0.906
dV	20.643	15.015	0.000
dQ	0.741	0.539	0.592
VQ	0.877	0.638	0.526

Table A-3. The test on individual coefficients for the model of standard deviation of fiber diameter (StdFD)

Term (coded)	Coef.	T	*p*-Value
Constant	36.1574	39.381	0.000
C	4.5788	12.216	0.000
D	−1.5536	−4.145	0.000
V	6.4012	17.078	0.000
Q	1.1531	3.076	0.003
C^2	−2.2937	−3.533	0.001
d^2	−0.1115	−0.172	0.864
V^2	−1.1891	−1.832	0.072
Q^2	3.0980	4.772	0.000
Cd	−0.2088	−0.455	0.651
CV	1.0010	2.180	0.033
CQ	2.7978	6.095	0.000
dV	0.1649	0.359	0.721
dQ	−2.4876	−5.419	0.000
VQ	1.5182	3.307	0.002

As depicted, the terms related to Q^2, CQ, dQ, and VQ in the model of MFD and related to d^2, Cd, and dV in the model of StdFD have very high *p*-values; therefore, they do not contribute significantly in representing the variation of the corresponding response. Eliminating these terms will enhance the efficiency of the models. The new models are then given by recalculating the unknown coefficients in terms of coded variables in Eqs. (A-13) and (A-14), and in terms of natural (uncoded) variables in Eqs. (A-15), (A-16).

$$\text{MFD}=281.755+34.953x_1+5.622x_2-2.113x_3+9.013x_4-11.613x_1^2 -4.304x_2^2-15.500x_3^2+12.517x_1x_2+4.020x_1x_3+20.643x_2x_3 \quad \text{(A-13)}$$

$$\text{StdFD}=36.083+4.579x_1-1.554x_2+6.401x_3+1.153x_4 -2.294x_1^2-1.189x_3^2+3.098x_4^2+1.001x_1x_3 +2.798x_1x_4-2.488x_2x_4+1.518x_3x_4 \quad \text{(A-14)}$$

Table A-4. Summary of the results from statistical analysis of the models after eliminating the insignificant terms

	F	*p*-Value	R^2	R^2_{adj}	R^2_{pred}
MFD	155.56	0.000	95.69%	95.08%	94.18%
StdFD	55.61	0.000	89.86%	88.25%	86.02%

$$\begin{aligned}MFD=&10.3345+48.7288C-22.7420d+7.9713V\\&+90.1250Q-2.9033C^2-0.1722d^2-0.6120V^2\\&+1.2517Cd+0.4020CV+0.8257dV\end{aligned} \quad \text{(A-15)}$$

$$\begin{aligned}StdFD=&-1.8823+7.5590C+1.1818d+1.2709V\\&-300.3410Q-0.5734C^2-0.0476V^2+309.7999Q^2\\&+0.1001CV+13.9892CQ-4.9752dQ+3.0364VQ\end{aligned} \quad \text{(A-16)}$$

The results of the test for significance as well as R^2, R^2_{adj}, and R^2_{pred} for the new models are given in Table A-4. It is obvious that the *p*-values for the new models are close to zero, indicating the existence of some significant terms in each model. Comparing the results of this table with Table A-1, the F statistic increased for the new models, indicating the improvement of the models after eliminating the insignificant terms. Despite the slight decrease in R^2, the values of R^2_{adj}, and R^2_{pred} increased substantially for the new models. As mentioned earlier, R^2 will always increase with the number of terms in the model. Therefore, the smaller R^2 values were expected for the new models, due to the fewer terms. However, this does not necessarily suggest that the previous models were more efficient. Looking at the tables, R^2_{adj}, which provides a more useful tool for comparing the explanatory power of models with different number of terms, increased after eliminating the unnecessary variables. Hence, the new models have the ability to better explain the experimental data. Due to higher R^2_{pred}, the new models also have higher prediction ability. Thus, eliminating the insignificant terms results in simpler models that not only present the experimental data in superior form, but also are more powerful in predicting new conditions.

The test for individual coefficients was performed again for the new models. The results of this test are summarized in Table A-5 and Table A-6. This time, as it was anticipated, no terms had higher *p*-value than expected, which needed to be eliminated. Here is another advantage of removing unimportant terms. The values of T statistic increased for the terms already in the models, implying that their effects on the response became stronger.

Table A-5. The test on individual coefficients for the model of mean fiber diameter (MFD) after eliminating the insignificant terms

Term (coded)	Coef.	T	*p*-Value
Constant	281.755	118.973	0.000
C	34.953	31.884	0.000
d	5.622	5.128	0.000
V	−2.113	−1.927	0.058
Q	9.013	8.221	0.000
C^2	−11.613	−6.116	0.000
d^2	−4.304	−2.267	0.026
V^2	−15.500	−8.163	0.000
Cd	12.517	9.323	0.000
CV	4.020	2.994	0.004
dV	20.643	15.375	0.000

Table A-6. The test on individual coefficients for the model of standard deviation of fiber diameter (StdFD) after eliminating the insignificant terms

Term (coded)	Coef.	T	*p*-Value
Constant	36.083	45.438	0.000
C	4.579	12.456	0.000
d	−1.554	−4.226	0.000
V	6.401	17.413	0.000
Q	1.153	3.137	0.003
C^2	−2.294	−3.602	0.001
V^2	−1.189	−1.868	0.066
Q^2	3.098	4.866	0.000
CV	1.001	2.223	0.029
CQ	2.798	6.214	0.000
dQ	−2.488	−5.525	0.000
VQ	1.518	3.372	0.001

After the relationship between parameters was developed, the test data were used to investigate the prediction ability of the models. Root mean square errors (RMSE) between the calculated responses (C_i) and real responses (R_i) were determined using Eq. (A-17) for experimental data as well as test data for the sake of evaluation of both MFD and StdFD models.

$$RMSE=\sqrt{\frac{\sum_{i=1}^{n}(C_i-R_i)^2}{n}} \quad \text{(A-17)}$$

REFERENCES

1. J. Doshi and D. H. Reneker, *J. Electrostatics*, **35**, 151 (1995).
2. H. Fong and D. H. Reneker, *Electrospinning and the formation of nanofibers*, in: D. R. Salem (Ed.), *Structure formation in polymeric fibers*, Hanser, Cincinnati (2001).
3. D. Li and Y. Xia, *Adv. Mater.*, **16**, 1151 (2004).
4. R. Derch, A. Greiner and J. H. Wendorff, *Polymer nanofibers prepared by electrospinning*, in: J. A. Schwarz, C. I. Contescu and K. Putyera (Eds.), *Dekker Encyclopedia of Nanoscience and Nanotechnology*, CRC, New York (2004).
5. A. K. Haghi and M. Akbari, *Phys. Stat. Sol. A*, **204**, 1830 (2007).
6. P. W. Gibson, H. L. Schreuder-Gibson and D. Rivin, *AIChE J.*, **45**, 190 (1999).
7. M. Ziabari, V. Mottaghitalab and A. K. Haghi, *Korean J. Chem. Eng.*, **25**, 923 (2008).
8. Z. M. Huang, Y. Z. Zhang, M. Kotaki and S. Ramakrishna, *Compos. Sci. Technol.*, **63**, 2223 (2003).
9. M. Li, M. J. Mondrinos, M. R. Gandhi, F. K. Ko, A. S. Weiss and P. I. Lelkes, *Biomaterials*, **26**, 5999 (2005).
10. E. D. Boland, B. D. Coleman, C. P. Barnes, D. G. Simpson, G. E. Wnek and G. L. Bowlin, *Acta. Biomater.*, **1**, 115 (2005).
11. J. Lannutti, D. Reneker, T. Ma, D. Tomasko and D. Farson, *Mater. Sci. Eng. C*, **27**, 504 (2007).
12. J. Zeng, L. Yang, Q. Liang, X. Zhang, H. Guan, C. Xu, X. Chen and X. Jing, *J. Control. Release*, **105**, 43 (2005).

13. E. R. Kenawy, G. L. Bowlin, K. Mansfield, J. Layman, D. G. Simpson, E. H. Sanders and G. E. Wnek, *J. Control. Release*, **81**, 57 (2002).
14. M. S. Khil, D. I. Cha, H.-Y. Kim, I.-S. Kim and N. Bhattarai, *J. Biomed. Mater. Res. Part B: Appl. Biomater.*, **67**, 675 (2003).
15. B. M. Min, G. Lee, S. H. Kim, Y. S. Nam, T. S. Lee and W. H. Park, *Biomaterials*, **25**, 1289 (2004).
16. X. H. Qin and S. Y. Wang, *J. Appl. Polym. Sci.*, **102**, 1285 (2006).
17. H. S. Park and Y. O. Park, *Korean J. Chem. Eng.*, **22**, 165 (2005).
18. J. S. Kim and D. H. Reneker, *Poly. Eng. Sci.*, **39**, 849 (1999).
19. S. W. Lee, S. W. Choi, S. M. Jo, B. D. Chin, D. Y. Kim and K. Y. Lee, *J. Power Sources*, **163**, 41 (2006).
20. C. Kim, *J. Power Sources*, **142**, 382 (2005).
21. N. J. Pinto, A. T. Johnson, A. G. MacDiarmid, C. H. Mueller, N. Theofylaktos, D. C. Robinson and F. A. Miranda, *Appl. Phys. Lett.*, **83**, 4244 (2003).
22. D. Aussawasathien, J.-H. Dong and L. Dai, *Synthetic Met.*, **54**, 37 (2005).
23. S.-Y. Jang, V. Seshadri, M.-S. Khil, A. Kumar, M. Marquez, P. T. Mather and G. A. Sotzing, *Adv. Mater.*, **17**, 2177 (2005).
24. S.-H. Tan, R. Inai, M. Kotaki and R. Ramakrishna, *Polymer*, **46**, 6128 (2005).
25. A, Ziabicki, *Fundamentals of fiber formation: The science of fiber spinning and drawing*, Wiley, New York (1976).
26. A. Podgóski, A. Bałazy and L. Gradoń, *Chem. Eng. Sci.*, **61**, 6804 (2006).
27. B. Ding, M. Yamazaki and S. Shiratori, *Sens. Actuators B*, **106**, 477 (2005).
28. J. R. Kim, S. W. Choi, S. M. Jo, W. S. Lee and B. C. Kim, *Electrochim. Acta*, **50**, 69 (2004).
29. L. Moroni, R. Licht, J. de Boer, J. R. de Wijn and C. A. van Blitterswijk, *Biomaterials*, **27**, 4911 (2006).